Hindawi Publishing Corporation
Advances in OptoElectronics
Volume 2007, Article ID 83657, 11 pages
doi:10.1155/2007/83657

Research Article

Rapid Thermal Annealing and Hydrogen Passivation of Polycrystalline Silicon Thin-Film Solar Cells on Low-Temperature Glass

Mason L. Terry, Daniel Inns, and Armin G. Aberle

Photovoltaics Centre of Excellence, The University of New South Wales, Sydney, NSW 2052, Australia

Received 24 April 2007; Revised 24 August 2007; Accepted 16 October 2007

Recommended by Xian An Cao

The changes in open-circuit voltage (V_{oc}), short-circuit current density (J_{sc}), and internal quantum efficiency (IQE) of aLuminum induced crystallization, ion-assisted deposition (ALICIA) polycrystalline silicon thin-film solar cells on low-temperature glass substrates due to rapid thermal anneal (RTA) treatment and subsequent remote microwave hydrogen plasma passivation (hydrogenation) are examined. V_{oc} improvements from 130 mV to 430 mV, J_{sc} improvements from 1.2 mA/cm^2 to 11.3 mA/cm^2, and peak IQE improvements from 16% to > 70% are achieved. A 1-second RTA plateau at 1000°C followed by hydrogenation increases the J_{sc} by a factor of 5.5. Secondary ion mass spectroscopy measurements are used to determine the concentration profiles of dopants, impurities, and hydrogen. Computer modeling based on simulations of the measured IQE data reveals that the minority carrier lifetime in the absorber region increases by 3 orders of magnitude to about 1 nanosecond (corresponding to a diffusion length of at least 1 μm) due to RTA and subsequent hydrogenation. The evaluation of the changes in the quantum efficiency and V_{oc} due to RTA and hydrogenation with computer modeling significantly improves the understanding of the limiting factors to cell performance.

1. INTRODUCTION

Thin-film solar cells are becoming increasingly attractive due to the limitations with silicon feedstock and the drive to lower the manufacturing cost and the final module cost. During the fabrication of thin-film silicon solar cells, very little silicon is used (typical film thickness of <10 μm) and the processing steps are of relatively low cost. As such, thin-film polycrystalline silicon (pc-Si) films on low-temperature glass substrates are ideally suited to achieve the goal of less than US$1 per Watt in a finished module.

In pc-Si thin-film solar cells, defect removal, defect passivation, and dopant activation are critical to device performance. Both point-like and extended defects are typically introduced during the fabrication of thin-film solar cells. Many of these defects generate recombination centers within the semiconductor bandgap, dramatically lowering the minority carrier lifetime. Removing and/or passivating these defects is required to obtain sufficiently high minority carrier lifetimes. This is done through thermal annealing and passivation techniques. A potential problem with thermal annealing of thin-film solar cells is extensive dopant diffusion ("smearing"), which can eventually lead to electrical shunting of the diode structure. A second problem arises when low-temperature substrates are used, thereby limiting annealing time and/or temperature.

Rapid thermal annealing (RTA) has replaced the tube furnace in many applications to perform high-temperature (>700°C) processing steps for defect annealing, dopant activation, and/or diffusion. RTA processes are ideally suited for thin-film pc-Si solar cells on glass substrates [1–3] as precise control of the thermal profile that the device sees is achieved. Fast temperature ramp rates limit the diffusion of dopants within the device, minimize glass damage all while achieving efficient defect removal. Hydrogen passivation (hydrogenation) is crucial in passivating extended and point-like defects. In thin-film devices, this hydrogenation is typically performed using an RF or microwave-powered hydrogen plasma. The open-circuit voltage (V_{oc}) of pc-Si thin-film solar cells on glass is typically more than doubled by the hydrogenation step [1–5].

Section 2 starts with a brief description of the investigated mesa-type solar cells and then describes the post-deposition processing systems, the different measurement

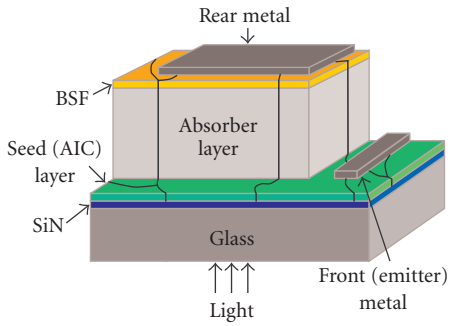

Figure 1: Mesa-type ALICIA cell structure as used in the present work.

techniques, and the sample fabrication processing used in this work. Section 3 first presents the experimental results obtained in this study, including Suns-V_{oc}, internal and external quantum efficiency (IQE, EQE), short-circuit current densities (J_{sc}) calculated from the measured EQE curves, and a summary of the electrical measurements. This is followed by secondary ion mass spectroscopy (SIMS) data and a discussion of the experimental results. Section 4 presents computer simulations of the investigated solar cells to determine their minority carrier lifetimes in the as-grown state, after a 1000°C RTA, and after a subsequent hydrogenation. Finally, Section 5 presents the conclusions from this study.

2. EXPERIMENTAL PARAMETERS

The aluminum induced crystallization, ion-assisted deposition (ALICIA) solar cell is well described in the literature [6, 7]. Figure 1 shows a Mesa-type version of this cell as used in the present paper. Planar Borofloat33 glass panes ($5 \times 5\,\text{cm}^2$, 3 mm thick) (Schott AG, Mainz, Germany) are used as substrates. An SiN:H layer with a thickness of ~75 nm is deposited by microwave plasma-enhanced chemical vapor deposition (PECVD). The seed layer (emitter) is formed by an aluminum-induced crystallization process (AIC) [8], giving pc-Si with a typical grain size of ~20 μm and a thickness of ~200 nm. The absorber (base) and back surface field (BSF) layers are then grown using ion-assisted deposition of e-beam evaporated Si and in-situ doping from effusion cells of gallium (Ga) and phosphorus (P). This gives the following structure: Glass (planar), SiN (75 nm), p^+ (AIC, 200 nm, $\sim 2 \times 10^{19}\,\text{cm}^{-3}$ Al), p^- (IAD, 50 nm, $\sim 1 \times 10^{17}\,\text{cm}^{-3}$ Ga), n^- (IAD, 1000 nm, $\sim 4 \times 10^{16}\,\text{cm}^{-3}$ P), n^+ (IAD, 100 nm, $N_{surface} = \sim 1 \times 10^{19}\,\text{cm}^{-3}$ P). The samples used in this study are nominally identical, with three mesa structures (two $1 \times 15\,\text{mm}^2$ strips and one $18 \times 14\,\text{mm}^2$ "square") per glass substrate that all receive identical processing apart from the RTA process. During the growth of the base and BSF layers, a mask is used to cover parts of the seed layer, forming a mesa structure via shadow-mask epitaxy. This enables a simple metallization of the device with Al contacts, as shown in Figure 1.

The RTA system used in this study is tungsten-halogen lamp based, uses an N_2 ambient at one atmosphere of pressure, and has a graphite plate to support the glass substrates. The time at plateau and cooling rate from plateau (either controlled cooling or natural cooling with no heating from plateau down to 650°C) is varied in this investigation. To perform the hydrogenation, a pulsed remote microwave plasma source is used in a cold wall reactor. The microwave power for this study is 3.2 kW, with a 30-second pulse length for both on and off. A pulsed mode is used to avoid overheating of the microwave generator. The hydrogenation plateau is 620°C for 15 minutes, using an H_2:Ar plasma. Then the glass temperature is reduced to 325°C over 14 minutes, the plasma is turned off, and the samples removed.

The 1-Sun V_{oc} (termed "V_{oc}" hereafter) is taken from quasisteady state V_{oc} measurements ("Suns- V_{oc} curves") [9], and the fit parameters V_1 and V_2 are determined using a 2-diode model with fixed ideality factors of $n = 1$ and $n = 2$, respectively, plus a shunt resistance. In fact, V_1 and V_2 are the 1-Sun V_{oc} of the $n = 1$ and $n = 2$ diodes, respectively. The crossing point V_x of the fitted $n = 1$ and $n = 2$ curves provides a single parameter to evaluate the relative importance of the recombination currents J_{01} and J_{02} [10]. If $V_{oc} = V_x$, then both recombination currents affect the 1-Sun V_{oc} equally. When V_x is greater than V_{oc} then the recombination current J_{02} becomes increasingly more important. As V_x becomes less than V_{oc} then J_{01} becomes increasingly dominant at V_{oc}. Additionally, V_2 needs to be 120 mV larger than V_{oc} to negligibly (<10%) contribute to the total recombination rate at V_{oc}. Generally, the $n = 2$ diode (J_{02}) accounts for recombination in the junction space charge region and at grain boundaries, whereas the $n = 1$ diode (J_{01}) accounts for bulk and surface recombination. The preferable recombination current dominance of V_{oc} is J_{01} to provide the best electrical performance at the maximum power point.

External quantum efficiency (EQE) measurements are performed on an Oriel system, with a wavelength step size of 5 nm. EQE(λ), the measure of electron flow under short-circuit conditions into the external circuit per photon incident onto the solar cell, can be converted to IQE(λ) if the total hemispherical reflectance $R(\lambda)$ and transmittance $T(\lambda)$ are known. IQE(λ) is then given by

$$\text{IQE}(\lambda) = \frac{\text{EQE}(\lambda)}{1 - R(\lambda) - T(\lambda)}. \quad (1)$$

A spectrometer (Varian Cary 5G) with integrating sphere is used to measure $R(\lambda)$ of the cell, with 1 nm steps from 300 nm to 1200 nm. Since the BSF layer in the entire probed sample region is coated with aluminum, no light will be transmitted; hence, $T(\lambda)$ is zero in this work. Note that this expression neglects optical absorption in the Al and glass, which in turn results in a lower bound for the IQE. A point to remember is that these mesa solar cells are planar and hence, despite the Al back reflector (about half of the 600 nm light reaches the Al which itself has been shown to absorb around 30% of this light [11]), feature poor light trapping.

The EQE and reflectance measurements are performed on the large mesa cell on each glass substrate, ensuring that the entire diameter of the entering monochromatic light beam falls onto the device under test (this prerequisite is not fulfilled by the two small, stripe-like mesa cells on each glass

substrate). The measured EQE data are then used to calculate the corresponding J_{sc} of the solar cell under 1-Sun illumination. This is achieved by integration of the product of the measured EQE curve and the photon density in the standard terrestrial solar spectrum (AM1.5G, 100 mW/cm^2). Note that, due to the very large series resistance of the large mesa solar cells (>100 Ω-cm^2), the short-circuit current calculated from the EQE curve is larger than the short-circuit current that would be measured under actual AM1.5G illumination.

The sequence of cell fabrication and measurements used for this study was as follows: after the formation of the seed layer, the mesa structure was grown and Suns-V_{oc} measurements were taken. Then the cell had Al contacts formed by evaporation using a shadow mask. After the deposition of Al on the "square-"shaped sample, a single V_{oc} measurement was performed to verify that good ohmic contact between the pc-Si and the Al was achieved (reduction in $V_{oc} \leq 5$ mV, no short-circuiting of the diode). Then reflectance and EQE measurements were performed, followed by the IQE calculation. Then the Al was chemically removed, the cell chemically cleaned, and the RTA process performed. The measurement and contact formation sequence were then repeated. The metal contacts were then removed and the cell cleaned, followed by a hydrofluoric acid dip in preparation for the hydrogenation sequence. After the hydrogenation process, the measurement and metal contact formation were repeated.

For the V_{oc} measurements, each of the samples had between 5 and 10 measurements before the Al deposition (with typically 2 per strip and 3 to 6 per "square"). This is to ensure good statistical accuracy in the measurement and to eliminate any cell that failed during the previous processing step. Additionally, all samples within a plateau time split (900°C and 1000°C groups) were all measured at one time to minimize any drift in the measurement systems.

3. EXPERIMENTAL RESULTS

3.1. Suns-V_{oc}

Figures 2 and 3 show the effect on V_{oc} and V_x before and after hydrogenation resulting from the variation in RTA plateau time at 900°C and 1000°C, respectively. RTA times at 900°C plateau temperature are as follows: no RTA, 30, 60, 135, 165, and 210 seconds. RTA plateau times at 1000°C plateau temperature are as follows: no RTA, 1, 10, 15, and 30 seconds. As might be expected, the V_{oc} increases, reaches a plateau, and then falls off, especially in the case of a 30-second, 1000°C RTA plateau where the V_{oc} is severely affected.

In Figure 2, 900°C RTA plateau, V_x is larger than V_{oc} after the RTA process, revealing that the samples are $n = 2$ dominated. It is noted that the measured value for the 135-second plateau sample had errors in 4 of the 5 measurements after RTA—this sample appears to have been damaged during processing and has therefore been eliminated from the study. At 60 seconds, average V_{oc} values of 236 mV and 399 mV before and after hydrogenation, respectively, are measured. The trend in V_{oc} after hydrogenation indicates that, for the

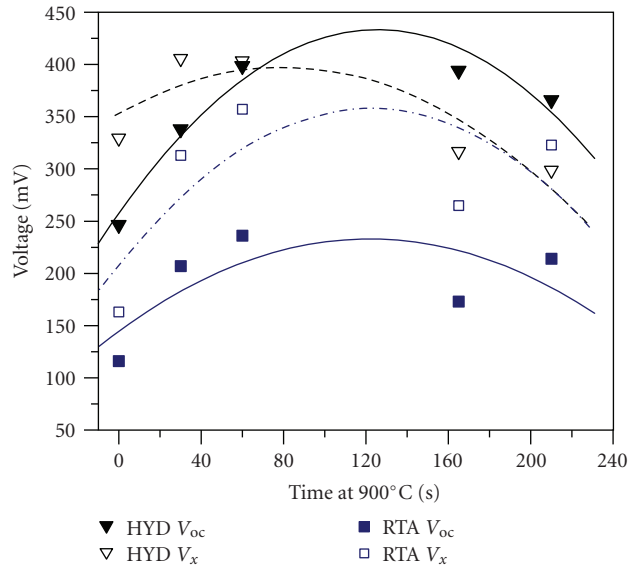

Figure 2: Measured V_{oc} and V_x following RTA and hydrogenation as a function of RTA plateau time at 900°C. The lines are second-order polynomial fits.

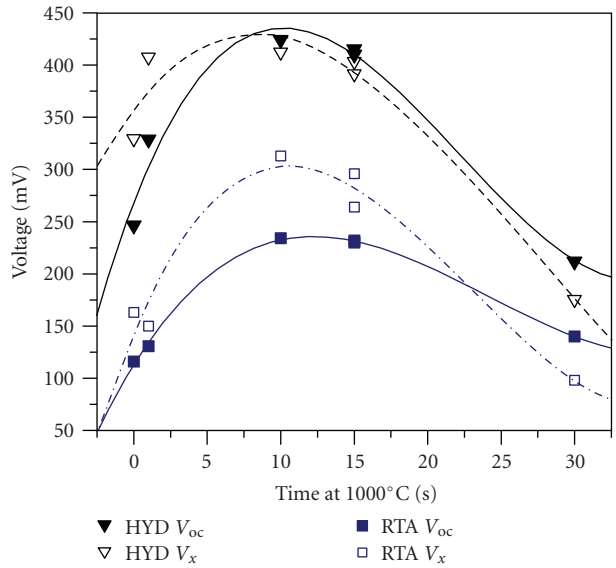

Figure 3: Measured V_{oc} and V_x following RTA and hydrogenation as a function of RTA plateau time at 1000°C. The lines are third-order polynomial fits.

900°C RTA, a maximum occurs between 60- and 165-second plateau time.

In Figure 3 it can be seen that for the 30-second RTA at 1000°C the device is drastically affected both before and after hydrogenation, most likely due to Al diffusion along grain boundaries (as explained later), causing shunting and drastic smearing of the junction. After the RTA treatment, V_x is greater than V_{oc} except in the case of a 30-second 1000°C RTA plateau. At around 10 seconds the V_{oc} maximizes to an average value of 235 mV and 425 mV before and after hydrogenation, respectively, and in the hydrogenated sample

is approximately equally affected by the two recombination currents.

The variation in V_x has some interesting characteristics that provide significant insight into what the limiting defects are in the cells. Before hydrogenation, V_{oc} is more J_{02} affected, as seen by V_x being greater than V_{oc} regardless of RTA temperature and time (except for the extreme case of a 1000°C, 30-second RTA). Following hydrogenation, V_x is still larger than V_{oc} for short RTA times ($\leq$30 seconds at 900°C and $\leq$1 second at 1000°C). The crossover point lies at around 70 seconds and 8 seconds for the 900°C and 1000°C RTA process, respectively. Below this crossover point the V_{oc} is mostly affected by J_{02} recombination. Above this crossover point the V_{oc} is slightly more affected by J_{01} recombination than J_{02} recombination in the case of the 1000°C RTA process, yet mostly affected by J_{01} recombination in the case of the 900°C RTA process.

3.2. Quantum efficiency

The effect of a 1000°C RTA process on the IQE of ALICIA cells is shown in Figure 4. Since these are planar multilayer thin-film diodes, there are interference fringes in the EQE and reflectance data. The IQE curve above about 500 nm is affected by light reflecting off of the back contact although, as noted earlier, a significant fraction of the light that reaches the Al back contact is absorbed by the Al. This reflected light effect is most apparent in the "as-grown" curve. Without an RTA the IQE peak sits at around 430 nm and then drastically drops at longer wavelengths, indicating very low effective lifetime of minority carriers in the absorber region. With an RTA the increase in total response is quite large over the entire range of relevant wavelengths (300–1100 nm), showing that the effective lifetimes in all device regions (emitter, junction depletion region, base) have been improved significantly by the RTA process. However, the peak IQE value of merely 40% after RTA shows that the IQE is still too low for efficient conversion of the solar spectrum.

Following hydrogenation for 15 minutes at 620°C, the increase in IQE from a peak of 40% to over 70% is seen (as in Figure 5), and good improvement over all other wavelengths also results. Thus, the effective lifetime in the absorber region is drastically improved by hydrogenation of the 1000°C RTA treated samples. Even with a 1-second RTA plateau time the quantum efficiency improves significantly. Looking at the peaks of the 1-, 10-, and 15-second curves, it can be seen that the longer RTA greatly improves the defect density within the junction and absorber regions, as indicated by the broadening and increased magnitude of the peak. Excessively long RTA times negatively affect the device, as confirmed by the 30-second 1000°C RTA process. Comparing the curves labeled "as-grown" and "no RTA with hydrogenation," a dramatic increase in the peak IQE from 16% to 41% is seen. Moving to longer wavelengths from the peak response, the effect on the absorber region is large in that effective minority carrier lifetime is greatly increased. This increased effective lifetime in the absorber region is thought to be due to an efficient passivation of the bulk defects and grain boundaries. Hydrogenation alone has at least as much impact on

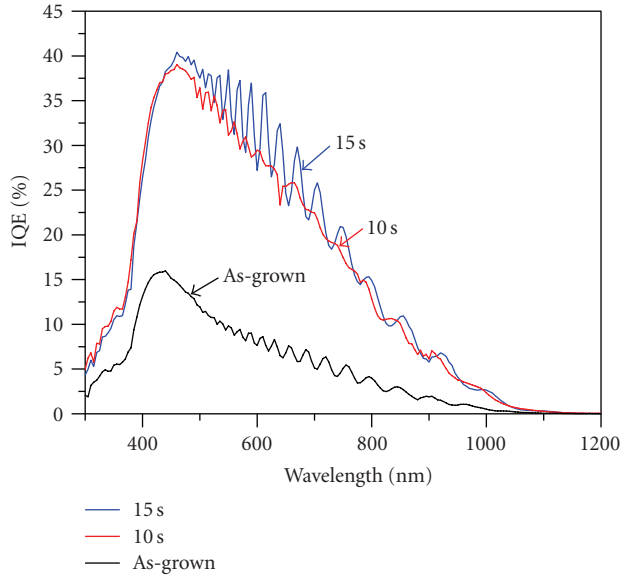

Figure 4: Measured IQE of ALICIA cells before and after the 1000°C RTA step. RTA plateau times are 10 and 15 seconds. The curve labeled as-grown is the best IQE measured in the course of this study on as-grown samples.

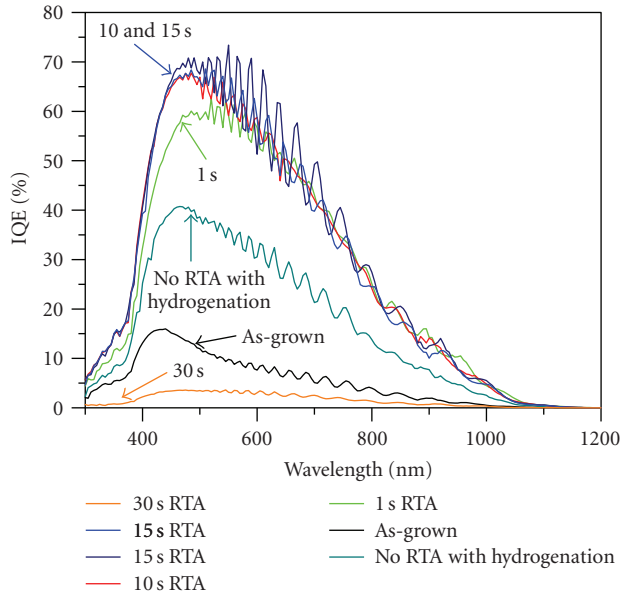

Figure 5: Measured IQE of hydrogenated ALICIA cells as a function of the 1000°C RTA plateau time. RTA plateau times are 1, 10, 15, and 30 seconds. Also shown, for comparison, are the IQE of the best as-grown cell and a hydrogenated cell that did not receive an RTA step.

the quantum efficiency of ALICIA solar cells as defect annealing although a combination of both gives the greatest benefit.

In Figure 6 the IQE evolution from the three processing steps for the cell that received a 15-second 1000°C RTA plateau is shown. As-grown, the IQE peaks at a rather poor value of 10% at a wavelength of 430 nm. Following the RTA, the peak IQE response is 40% at 460 nm, with good

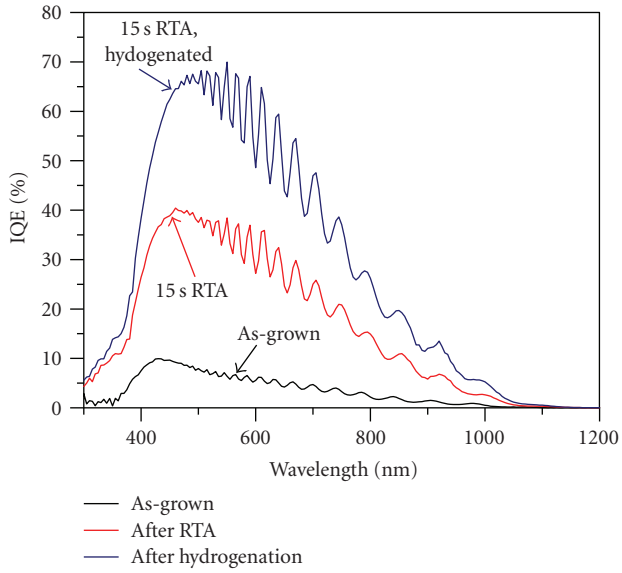

FIGURE 6: Measured improvement of the IQE of an ALICIA cell due to a 15-second 1000°C RTA process and a subsequent hydrogenation process.

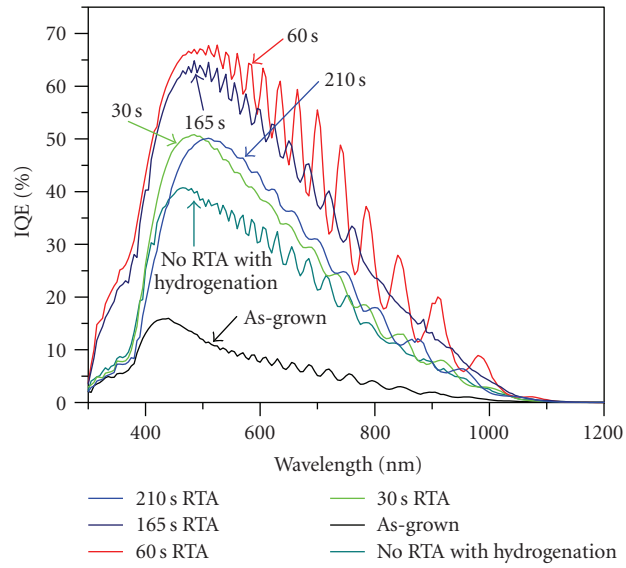

FIGURE 7: Measured IQE of hydrogenated ALICIA cells as a function of the 900°C RTA plateau time. RTA plateau times are 30, 60, 165, and 210 seconds. Also shown, for comparison, are the IQE of the best as-grown cell and a hydrogenated cell that did not receive an RTA step.

improvement in all wavelengths. With a subsequent hydrogenation, the peak IQE response is 68% at 490 nm with significant improvement over all wavelengths. The RTA and subsequent hydrogenation treatment improves the peak IQE value by a factor of 6.8 compared to the as-grown device.

Figure 7 shows the IQE response of hydrogenated samples to RTA plateau time at 900°C. As the RTA plateau time is increased, the peak response moves to longer wavelengths (from around 430 nm as-grown to about 500 nm with a 210-second RTA plateau time). A 60-second RTA plateau time at 900°C shows the best peak response of about 68%. The same IQE trend seen in the 1000°C samples is also seen with a 900°C RTA although differences do exist, namely the large increase in quantum efficiency below 400 nm for two of the cells and relatively modest improvement in the absorber region for the 30-second RTA cell.

3.3. Short-circuit current

Using the measured EQE curves, J_{sc} values for 1-Sun illumination (AM1.5G) can be determined for each cell. Determining the J_{sc} from the IQE is due to the contacts being optimized for IQE measurements. Figure 8 shows the J_{sc} results of hydrogenated samples as a function of the 900°C RTA plateau time. Also shown in this graph are the V_{oc} results of these samples. Figure 9 shows the corresponding graph for the samples that received a 1000°C RTA process. As expected, for both RTA plateau temperatures, the J_{sc} increases initially, then reaches a maximum, and eventually falls off with increasing RTA plateau time. The IQE evolution of a single cell as it moves through the fabrication stages (see, e.g., Figure 6) has a corresponding J_{sc} evolution of 1.2, 6.1, and 10.5 mA/cm^2, respectively, before the RTA process (i.e., as-grown), after the RTA process, and after subsequent hydrogenation. The maximum measured J_{sc} are 11.3 mA/cm^2 and 10.95 mA/cm^2 for the 900°C and 1000°C RTA process. Interestingly, the J_{sc} follows the same trend as the V_{oc} with respect to the RTA plateau time, and hence the product $J_{sc} \times V_{oc}$ has a sharp peak at the optimal RTA plateau time. From Figures 8 and 9 it follows that the optimal RTA plateau times are about 110 and 11 seconds, respectively, for the 900°C and 1000°C RTA process. With the addition of a good light

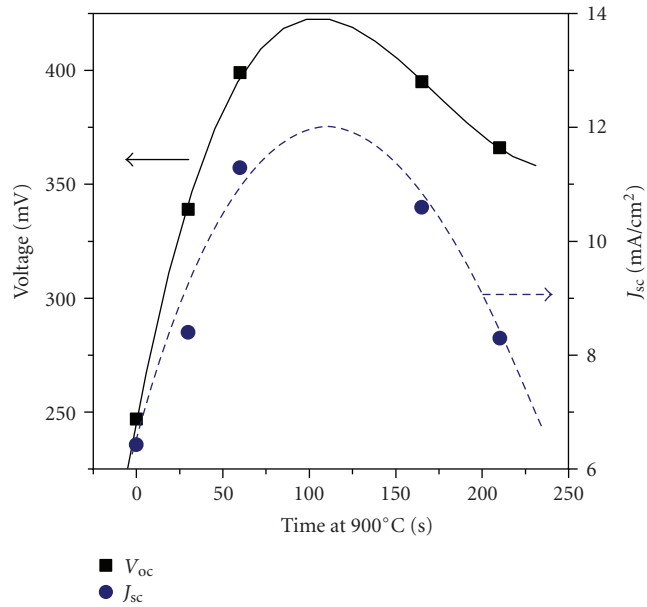

FIGURE 8: V_{oc} and J_{sc} evolution for a 900°C RTA plateau after hydrogenation. Lines are third-order polynomial fits.

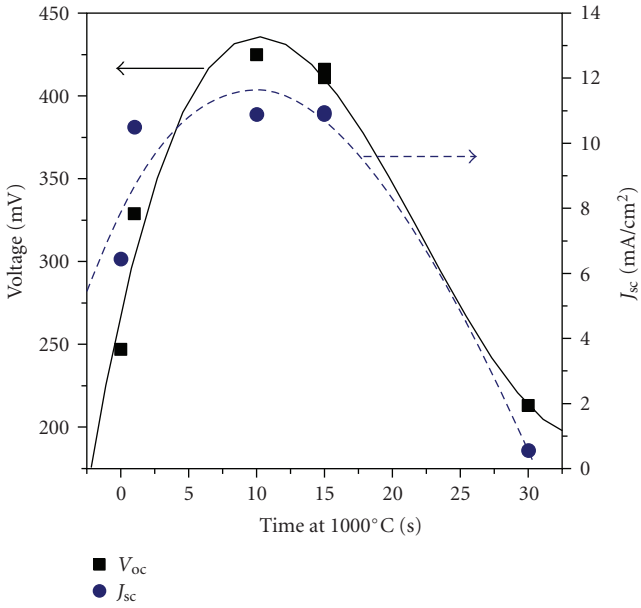

FIGURE 9: V_{oc} and J_{sc} evolution for a 1000°C RTA plateau after hydrogenation. Lines are third-order polynomial fits.

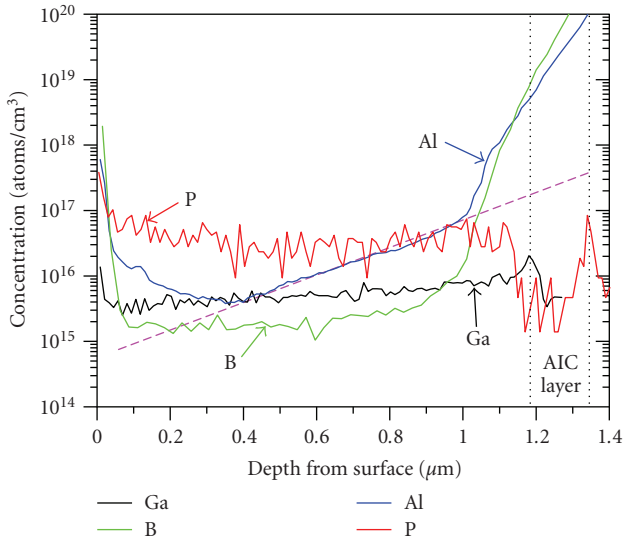

FIGURE 10: SIMS measurement of dopant atoms in the hydrogenated cell that received a 60-second RTA plateau time at 900°C. The dashed line is the estimated Al concentration due to Al diffusion along grain boundaries and in the bulk, as explained in Section 3.6.

trapping scheme such as described in [12, 13], much higher J_{sc} would result and this is presently being applied to the thin-film solar cells under development in our group.

3.4. Summary of electrical measurements

A summary of the measured effects of RTA plateau times at 900°C and 1000°C on peak IQE, J_{sc}, and V_{oc} is shown in Table 1. For comparison, the best as-grown cell and a hydrogenated cell that did not receive an RTA process are shown in the first subsection. In the second subsection, the measured electrical parameters are shown for the cell of Figure 6. The impact on J_{sc} from only the 15-second 1000°C RTA is enormous, from 1.2 mA/cm^2 to 6.11 mA/cm^2, a gain of 5, while the V_{oc} doubles to 230 mV. Similar gains in J_{sc} and V_{oc} are seen for the cell that received only a hydrogenation (i.e., no RTA), from 1.91 mA/cm^2 to 6.43 mA/cm^2 and 119 mV to 247 mV, respectively. With only a 1-second 1000°C RTA plateau time and hydrogenation, the majority of gain in J_{sc} is achieved, yet to maximize V_{oc} a much longer RTA plateau time is needed.

As seen from Table 1, the optimal RTA time for this solar cell structure is between 10 and 15 seconds at 1000°C to provide the best gain combination in J_{sc} and V_{oc}. The best V_{oc} measured within this study is 430 mV, which was obtained with a 10-second, 1000°C RTA plateau. The best J_{sc} measured within this study is 11.3 mA/cm^2, obtained with a 60-second 900°C RTA plateau. Note that natural cooling (lamps are turned off for the cooling phase from 1000°C to 650°C) also results in better IQE, V_{oc}, and J_{sc}, most likely due to slightly less time at 1000°C.

3.5. SIMS

After the completion of the above quantum efficiency measurements, two samples (60 seconds at 900°C and 10 seconds at 1000°C) were selected, the metal contacts removed, and the samples submitted to SIMS measurements. SIMS was performed by Evans Analytical Group (Calif, USA) using Si standards to measure the requested elements with a concentration accuracy typically within ± 20%. The area of the measured spot was about 100 μm × 100 μm in each SIMS run. On each sample two SIMS runs were performed on adjacent areas, giving the concentration profiles of the following elements: Al, B, Ga, and P. An additional SIMS measurement was performed on the 1000°C RTA sample to obtain its C, H, N, and O concentrations. Figure 10 shows the measured density of the dopant atoms in the cell that received a 60-second RTA plateau time at 900°C, while Figure 11 shows the corresponding data for the sample that received a 10-second RTA plateau time at 1000°C.

It is noted that the Al analysis is quite complex due to two different reasons: preferential sputtering during SIMS along the grain boundaries and Al inclusions in the AIC layer. Preferential sputtering at grain boundaries, a known effect in large-grained pc-Si, is due to atoms being removed faster at grain boundaries than intragrain, resulting in a nonplanar exposed sample surface. As the sputtering proceeds, the exposed surface becomes more nonuniform. This effect is supported by the order of increase in concentration of Al, N, C, and B (see Figures 11 and 12) as the exposed surface approaches the AIC interface. Al inclusions, a parasitic by-product of the AIC process, are preferentially located at grain boundaries (see Figure 13) and interrupt the uniformity of the seed layer laterally. An SIMS measurement on an ALICIA cell in Straub et al. [7] shows the complication of the Al concentration and the p-n junction profile due to what is thought to be from both effects. Both of these effects greatly

Table 1: Electrical characteristics of ALICIA cells as a function of the RTA plateau time. For comparison, the best as-grown cell and a hydrogenated cell that did not receive an RTA process are shown in the first subsection. Additionally, the electrical results of the cell measured in Figure 6 are shown in the second subsection. "ctrl." means controlled cooling (lamps on) from plateau, while "natural" means the lamps are set to minimum power until the temperature has dropped to 650°C.

RTA temp. (°C)	RTA time (s)	Peak IQE (%)	J_{sc} (mA/cm^2)	Average V_{oc} (mV)
N/A	N/A (as-grown)	16	1.91	119
N/A	N/A (no RTA, hydrogenated)	41	6.43	247
N/A	N/A (as-grown)	10	1.2	110
1000	15 (RTA only)	40	6.11	230
1000	Hydrogenated	68	10.87	411
900	30, ctrl. cool	51	8.41	339
900	60, ctrl. cool	68	11.30	399
900	165, ctrl. cool	65	10.55	395
900	210, ctrl. cool	50	8.34	366
1000	1, ctrl. cool	61	10.50	329
1000	10, ctrl. cool	67	10.90	425
1000	15, natural cool	71	10.95	416
1000	15, ctrl. cool	68	10.87	411
1000	30, ctrl. cool	3.6	0.56	213

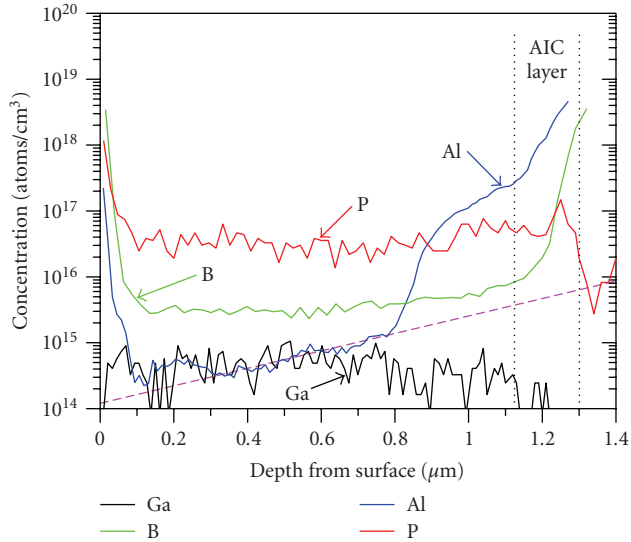

Figure 11: SIMS measurement of dopant atoms in the hydrogenated cell that received a 10-second RTA plateau time at 1000°C. The dashed line is the estimated Al concentration due to Al diffusion along grain boundaries and in the bulk, as explained in Section 3.6.

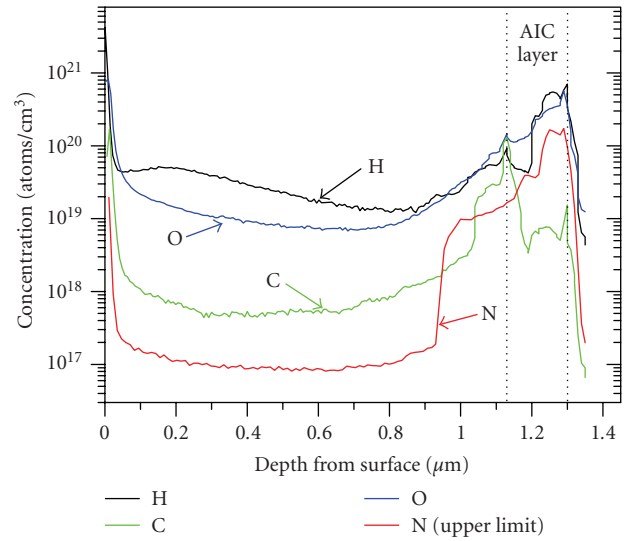

Figure 12: SIMS measurement of impurities and hydrogen in the hydrogenated cell that received a 10-second RTA plateau time at 1000°C.

complicate the analysis and require care in the SIMS interpretation.

The Al profile is significantly different in the two cells. In the sample that received the 900°C RTA, the maximum Al concentration in the AIC layer is about 9.5×10^{19} cm^{-3}, compared to 6.5×10^{18} cm^{-3} for the 1000°C sample. The Al concentration in the AIC layer of the 900°C sample is significantly higher than that of earlier SIMS results on ALICIA cells without Al inclusions [14] which showed a peak value of about 2×10^{19} cm^{-3}. In contrast, the Al concentration of the 1000°C sample is about 2 times lower. This indicates that the SIMS results from AIC seed layers must be taken with care.

The Al profiles indicated by the dashed straight lines in Figures 10 and 11 are due to diffusion of Al from the AIC layer during both growth of the absorber (Al is mobile at the temperatures used for growth) and the RTA process. This Al diffusion occurs both along grain boundaries and into the bulk of the grains. A 4-minute 900°C RTA process has previously been shown to increase the Al concentration within the absorber region of ALICIA cells by a factor of 10^7. The concentration of Al in the absorber region of the cell that

received the 900°C RTA plateau is dangerously high with respect to absorber dopant density and *p-n* junction profile. In contrast, in the cell that received the 1000°C RTA plateau, the Al concentration is more than a factor of 10 lower and well below the P concentration until the junction region is reached. At a depth of 0.8 μm in the absorber region, the concentration of Al is 2.4×10^{16} cm^{-3} and 1.5×10^{15} cm^{-3} for the 900°C and 1000°C RTA plateau cells, respectively.

Gallium does not incorporate well into the crystal structure during growth (due to its high mobility at the temperatures used during growth of ALICIA samples [7, 15]) and has virtually no effect on the actual doping of the samples. In the cell that received the 1000°C RTA plateau, Ga is near the detection limit of SIMS and around a factor of 10 lower than in the cell that received the 900°C RTA plateau.

The phosphorus-doped BSF layer of the SIMS samples is thinner than intended, which is due to (i) several sulfuric acid/hydrogen peroxide cleans and several HF dips between the various fabrication and measurement steps, (ii) the limited temperature ramp rate of our P effusion cell, and (iii) SIMS surface-related artefacts. Hot-probe measurements show that the surfaces of the samples are *n*-type. P concentration within the absorber region is as expected, about 4×10^{16} cm^{-3}, and uniform. Figures 10 and 11 show that P smearing from the BSF layer into the absorber region of ALICIA cells is negligible for the two RTA processes examined by SIMS (60 seconds at 900°C and 10 seconds at 1000°C).

The differences in the B profiles of Figures 10 and 11 have yet to be fully explained. Again, preferential sputtering during SIMS along the grain boundaries and Al inclusions in the AIC layer complicate the analysis. The concentration of B in the absorber region is similar yet significantly different in the AIC layer and near the junction region.

The concentration of H in Figure 12 shows substantial penetration throughout the cell structure. A minimum concentration of 2×10^{19} cm^{-3} is located near the *p-n* junction. In the first 200 nm of the cell, the H profile is approximately constant. A maximum of 1.3×10^{20} cm^{-3} is seen within the emitter, however, this concentration must be taken with care due to the SIMS artefacts at this depth.

The concentration of O within the entire cell structure is relatively high, about one order of magnitude higher than in Cz grown Si (approx. 1×10^{18} cm^{-3}) and about two orders of magnitude higher than in a previously published ALICIA SIMS measurement [7]. This previously published result was obtained on an ALICIA cell before an RTA treatment. While this sample showed that the O contamination during our non-UHV silicon epitaxy process can be kept at low levels, it is not representative for the O content of actual ALICIA cells after RTA. The high O content of the sample of Figure 12 is believed to be due to the RTA process.

The amount of C in the absorber region is around 5×10^{17} cm^{-3} as compared to the concentration of about 1×10^{16} cm^{-3} in a Cz Si wafer. The C profile shows a pronounced peak of about 1×10^{20} cm^{-3} at the original AIC surface. The N concentration in the absorber region is relatively low (about 1×10^{17} cm^{-3}) although does rise substantially at a depth of 0.93 μm from the surface, just after the rise in Al at 0.8 μm. This sharp rise in N is believed to be due to the same reasons that cause the complications with the Al profile (i.e., enhanced sputtering rate along grain boundaries and Al inclusions).

3.6. Discussion

Based on the above results, conclusions can be drawn that further explain the effects that are seen from RTA and hydrogenation. One possible reason for the relatively modest improvement of the IQE around 500 nm for the 30-second 900°C RTA cell (see Figure 7) is the combination of the junction space charge region still being near the absorber/AIC interface (which is thought to have a large density of defects and impurities, especially C as shown in Figure 12) and also the need for additional grain boundary improvement through secondary grain growth (removing the assumed confined amorphous layer along grain boundaries, see [16–18]). It is possible that some amorphous Si exists in the grain boundaries after an ALICIA cell has been grown. During the RTA, this amorphous material is incorporated into the grains as the grains grow to minimize grain boundary area (reduction in overall energy [16]), shrinking, and eventually eliminating the amorphous layer. Lateral conduction is also increased by this process. Additionally, small poor-quality grains have been seen to exist between the larger-gained material in ALICIA samples. Hydrogenation further improves the cell performance by passivating dangling bonds and impurities within the cell. By passivating the dangling bonds at the grain boundaries, the width of the depletion region surrounding each grain boundary is reduced, increasing lateral conduction and reducing recombination in the entire cell.

The shift of the wavelength corresponding to the peak of the IQE curve from around 430 to around 470 nm for the 1000°C sample (see Figure 5) and the broadening of the peak response provide some idea of the smearing of the junction from emitter diffusion deeper into the absorber region as verified by SIMS. Diffusion of dopants from the AIC layer deeper into the absorber region moves the *p-n* junction away from the defected and contaminated absorber/AIC interface, also reduce recombination. As such, the initial Si crystal growth quality on the epitaxy interface must be improved along with minimizing the impurity concentration to achieve better device performance. The RTA plateau time might then be reduced to limit the diffusion of Al into the absorber region, resulting in a narrower emitter and lower Al concentration in the absorber. A thinner seed layer would help with blue response by having a much narrower dead layer (emitter).

From the Suns-V_{oc} measurements and the J_{sc} values calculated from the measured EQE (see Figures 8 and 9), the optimal RTA plateau times are about 100 and 10 seconds for the 900°C and 1000°C RTA process, respectively. The solar cell efficiency is furthermore affected by the fill factor (FF) of the current-voltage curve. Given that $n = 1$ recombination produces higher FF values than $n = 2$ recombination, the optimum RTA time is also affected by the diode's ideality factor near the 1-Sun maximum power point. The maximum power point voltage is approximately equal to the V_{oc}

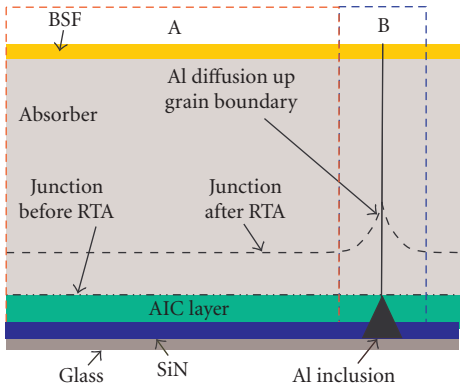

FIGURE 13: Schematic representation of *p-n* junction location before and after RTA, including enhanced diffusion of Al along a grain boundary. The areas denoted as "A" and "B" refer to the intragrain region and grain boundary region, respectively. An Al inclusion is shown which can exist in the AIC layer at the grain boundary. Drawing not to scale.

measured at a light intensity of 0.1 Suns. In terms of V_x, the optimal FF is thus realized for the situation where the 1-Sun V_{oc} is much larger than V_x. As can be seen from Figures 2 and 3, this slightly increases the optimal RTA plateau time for both investigated RTA temperatures. With respect to solar cell efficiency, the two RTA plateau temperatures investigated are performing approximately equally, with the hotter RTA process (~11 seconds at 1000°C) giving better V_{oc} but slightly lower J_{sc} and FF than the colder RTA process (~110 seconds at 900°C).

Enhanced diffusion of Al along grain boundaries of ALICIA material due to the RTA process has recently been confirmed by Inns and Campbell [19] where the *p-n* junction is shown to extend along a grain boundary using high-resolution electron-beam-induced current measurements. A schematic representation of this effect is shown in Figure 13 where there is enhanced diffusion along the grain boundary in region "B" in contrast to normal diffusion in region "A." Al is the fastest diffuser of the typical dopants in Si [15, 20] and especially in the open structure of grain boundaries in pc-Si [16]. The depth of enhanced diffusion down grain boundaries compared to intragrain diffusion has been shown to be inversely dependent upon temperature, that is, a hotter RTA process results in a shallower diffusion depth in the grain boundary [21, 22]. The enhanced diffusion is dependent upon the grain boundary properties such as width of the grain boundary, diffusivity within the grain, and diffusivity from the grain boundary into the grain. The inverse temperature dependence reported in the literature for this effect is confirmed by our results, that is, much lower concentration of Al in the absorber region as shown by the dashed lines in Figures 10 and 11 and a sharper rise in Al at around 0.8 μm in depth for the 1000°C RTA plateau sample. The analysis is quite complicated due to preferential sputtering and Al inclusions. The determination of the diffusivity within grains and along grain boundaries for the ALICIA cell is ongoing and includes effects such as dopant and impurity segregation to grain boundaries and secondary grain growth.

The differences in the B profiles in/near the AIC layers in the two SIMS results (see Figures 10 and 11) are very likely due to the same reasons that caused the artefacts in the Al profiles and thus should be ignored. Similarly, the high boron concentration in the BSF layer is very likely a surface-related artefact of the SIMS measurements (it is well known that the results from the first ~50 nm of probed material should not be trusted in standard SIMS). We have verified the doping polarity of the exposed surface region of our samples with hot-probe measurements, and the clear result was that the surface region is *n*-type. The B peak near the SiN interface is thought to come from the borosilicate glass substrate (Borofloat33).

Oxygen is well known to be a thermal donor in Si and forms at least eight different thermal donor species during annealing at 450°C with additionally reported donor formations for heat treatments between 550°C and 800°C. Oxygen is easily passivated by H which forms a stable bond up to above 400°C. In this study, the high concentration of O seems to have been well passivated resulting in substantial V_{oc} and J_{sc} gains due to hydrogenation.

It has been reported that even a thin heavily doped *n*-type layer greatly impedes H diffusion into *p*-type Si [23], however, in ALICIA material this seems not to be a problem. The most likely reason for the very effective hydrogenation of our samples is the high sample temperature (260°C) and the high plasma power (3.2 kW) used during the process. The grain boundaries could also play a role in this, as they are known to provide a pathway for enhanced diffusion of H into pc-Si films [23, 24], although this effect is dependent upon grain boundary properties. The relatively fast rise in the concentration of both H and N encountered in the emitter region supports preferential grain boundary sputtering. The SiN layer has a high concentration of both H and N which is seen well before the AIC/glass interface.

4. COMPUTER MODELING

To determine the effect of the different solar cell processing steps on the minority carrier lifetimes in the devices, the one-dimensional semiconductor simulator PC1D [25] is used to fit the measured IQE and J_{sc}. For these fits, a two-region device (vertical stack) is used where region 1 is a low-lifetime region simulating the highly defective pc-Si of the AIC layer and the interface region (which together form most of the emitter of the ALICIA cell) and region 2 encompasses the remaining emitter region (formed by diffusion of Al), the base, and the BSF layer. Doping profiles are designed to approximate the results obtained from the SIMS measurements using a combination of Gaussian and erfc profiles for the emitter and *p-n* junction, while an erfc profile is used for the BSF. The depth of the *p-n* junction below the cells' illuminated surface is varied until good agreement between measured and fitted peak IQE values is obtained. The material parameters of single-crystal Si were assumed. Other selected PC1D parameters include: internal reflectance front surface = 80%, rear surface = 67%; rear external reflectance = 95%; and front surface recombination $S_n = S_p = 90000$ cm/sec. The main fit parameters in

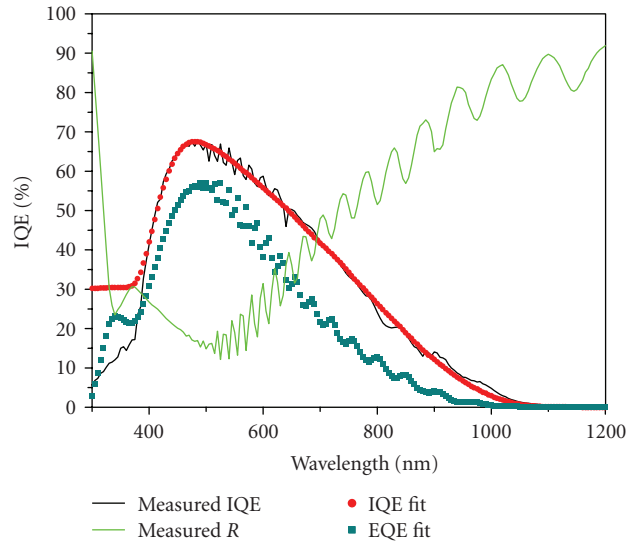

Figure 14: PC1D fit to the measured IQE and reflectance of an ALICIA cell.

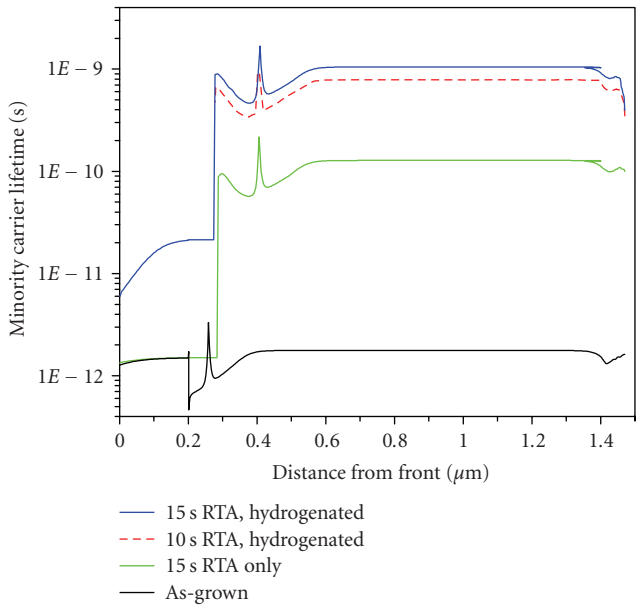

Figure 15: Evolution of the minority carrier lifetimes in ALICIA cells due to 1000°C RTA treatment and subsequent hydrogenation, as determined by PC1D analysis of measured IQE curves.

these PC1D simulations are the defect- (i.e., Shockley-Read-Hall recombination) related bulk lifetimes in the two regions. The mobility of free carriers in pc-Si materials is significantly lower than in high-purity single-crystal Si and is dependant on grain size and grain boundary properties [18, 26]. Due to the assumption of single-crystal silicon mobility values in the PC1D simulations, the lifetimes obtained are lower bounds to the actual lifetimes. It is noted that the crystal grains of ALICIA cells are pancake-like (i.e., the grain size is typically much larger than the film thickness) and hence the above PC1D simulations of the cells' short-circuit currents are representative of region A in Figure 13. An IQE fit to the measured data using PC1D is shown in Figure 14.

Figure 15 shows the evolution of the minority carrier lifetimes in ALICIA cells due to a 15-second RTA treatment at 1000°C and subsequent hydrogenation, as determined by PC1D analysis of measured IQE curves. Also shown, for comparison, is the carrier lifetime of a hydrogenated sample that received a 10-second RTA at 1000°C (dashed line). As can be seen from these PC1D results, the 1000°C RTA process improves the minority carrier lifetime in the base region of the investigated cells by about 2 orders of magnitude. Subsequent hydrogenation provides a further one order of magnitude improvement of the minority carrier lifetime to a value of about 1 nanosecond, which corresponds to a lower bound for the diffusion length in the base region of about 1000 nm.

5. CONCLUSION

In this paper the impact of rapid thermal annealing at 900°C and 1000°C and subsequent hydrogenation at 620°C on ALICIA pc-Si thin-film solar cells on low-temperature glass has been investigated experimentally. A strong increase in V_{oc} from 120 mV to 430 mV, J_{sc} from 1.2 mA/cm^2 to 11.3 mA/cm^2, and peak IQE from 16% to >70% in the best devices has been achieved. The effect of hydrogenation in removing defects that limit the current and voltage of the cells is enormous, resulting in a gain in J_{sc} of a factor of over 3 from hydrogenation alone. A 1-second RTA at 1000°C followed by a hydrogenation process increases the J_{sc} by more than a factor of 5. From the behavior of the cell voltages (V_{oc}, V_x) it follows that the RTA greatly reduces the density of grain boundary and space charge region defects, while hydrogenation is extremely effective in passivating grain boundaries, surfaces, and bulk defects of various sorts. As the RTA plateau time is increased, the evolution in defect density is seen in both Suns-V_{oc} and IQE measurements. Smearing of the junction space charge region is thought to mostly be from the diffusion of Al along-grain boundaries, limiting the RTA time at 900°C and 1000°C to $\leq$ 165 seconds and $\leq$ 15 seconds, respectively. Both V_{oc} and J_{sc} reach a maximum with the same RTA plateau time, for both RTA plateau temperatures investigated. SIMS measurements confirm that grain boundary diffusion is greatly reduced for the 1000°C RTA process compared to the 900°C process, although the time at plateau temperature is limited to 15 seconds as seen by the drastic reduction in electrical properties with a 30-second, 1000°C RTA plateau. Using PC1D simulations, minority carrier lifetime in the absorber region is shown to increase by about 3 orders of magnitude to a value of about 1 nanosecond due to RTA and subsequent hydrogenation, which corresponds to a diffusion length of at least 1 μm in the final devices. The evaluation of the passivation of defects has led to a better understanding of the factors limiting the performance of present ALICIA cells, paving the way towards ALICIA cells with a V_{oc} greater than 500 mV and a J_{sc} above 15 mA/cm^2.

ACKNOWLEDGMENTS

This work has been supported by the Australian Research Council. M. L. Terry and D. Inns acknowledge Ph.D. scholarships from UNSW. The authors would like to thank all group members that have contributed to the present state of the ALICIA cell technology.

REFERENCES

[1] M. L. Terry, A. Straub, D. Inns, D. Song, and A. G. Aberle, "Large open-circuit voltage improvement by rapid thermal annealing of evaporated solid-phase-crystallized thin-film silicon solar cells on glass," *Applied Physics Letters*, vol. 86, no. 17, Article ID 172108, 1–3, 2005.

[2] M. L. Terry, P. I. Widenborg, O. Kunz, and A G. Aberle, "Effects of Rapid thermal annealing and hydrogen passivation on crystalline silicon thin-film solar cells on glass made by PECVD solid-phase crystallization," in *Proceedings of Technical Digest of 15th International Photovoltaic Science & Engineering Conference (PVSEC '05)*, pp. 905–906, Shanghai, China, October 2005.

[3] M. L. Terry, D. Inns, and A G. Aberle, "Massive improvement through rapid thermal annealing and hydrogen passivation of pc-Si thin-film solar cells on glass based on aluminum induced crystallization," in *Proceedings of the IEEE 4th World Conference on Photovoltaic Energy Conversion*, pp. 1560–1563, Waikoloa, Hawaii, USA, May 2006.

[4] M. I. Keevers, A. Turner, U. Schubert, P. A. Basore, and M. A. Green, "Remarkably effective hydrogenation of crystalline silicon on glass modules," in *Proceedings of the 20th European Photovoltaic Solar Energy Conference (PVSEC '05)*, pp. 1305–1308, Barcelona, Spain, June 2005.

[5] A. Slaoui, E. Pihan, I. Ka, N. Mbow, S. Roques, and J. Koebel, "Hydrogen induced passivation of fine-grained polycrystalline silicon films," in *Proceedings of the Tecnical Digest of 15th International Photovoltaic Science & Engineering Conference (PVSEC '05)*, pp. 951–952, Shanghai, China, October 2005.

[6] A. G. Aberle, A. Straub, P. I. Widenborg, A. B. Sproul, Y. Huang, and P. Campbell, "Polycrystalline silicon thin-film solar cells on glass by aluminium-induced crystallisation and subsequent ion-assisted deposition (ALICIA)," *Progress in Photovoltaics: Research and Applications*, vol. 13, no. 1, pp. 37–47, 2004.

[7] A. Straub, D. Inns, M. L. Terry , R. Gebs, and A G. Aberle, "The influence of defects and postdeposition treatments on the free carrier density in lightly phosphorus-doped large-grained polycrystalline silicon films," *Journal of Applied Physics*, vol. 98, no. 2, Article ID 023507, 7 pages, 2005.

[8] P. I. Widenborg and A. G. Aberle, "Surface morphology of poly-Si films made by aluminium-induced crystallisation on glass substrates," *Journal of Crystal Growth*, vol. 242, no. 3-4, pp. 270–282, 2002.

[9] R. A. Sinton and A. Cuevas, "A quasi-steady-state open-circuit voltage method for solar cell characterization," in *Proceedings of 16th European Photovoltaic Solar Energy Conference*, pp. 1152–1155, Glasgow, UK, 2000.

[10] O. Kunz, D. Inns, A. B. Sproul , and A. G. Aberle, "Application of suns-voc and jsc-suns measurements to the characterization of mesatype thin-film solar cells," in *Proceedings of 21st European Photovoltaic Solar Energy Conference and Exhibition*, pp. 374–377, Dresden, Germany, September 2006.

[11] D. Inns, T. Puzzer, and A. G. Aberle, "Localisation of the p-n junction in poly-silicon thin-film diodes on glass by high-resolution crosssectional EBIC imaging," *Thin Solid Films*, vol. 515, no. 7-8, pp. 3806–3809, 2007.

[12] N. Chuangsuwanich, P. I. Widenborg, P. Campbell, and A. G. Aberle, "Light trapping properties of thin silicon films on AIT-textured glass," in *Proceedings of the Technical Digest 14th International Photovoltaic Science and Engineering Conference (PVSEC '04)*, pp. 325–326, Bangkok, Thailand, January 2004.

[13] A. G. Aberle, P. I. Widenborg, and N. Chuangsuwanich, "Glass texturing," International PCT patent application PCT/AU2004/000339, 2004.

[14] O. Nast and S. R. Wenham, "Elucidation of the layer exchange mechanism in the formation of polycrystalline silicon by aluminum-induced crystallization," *Journal of Applied Physics*, vol. 88, no. 1, Article ID 124132, 124–132, 2000.

[15] S. K. Ghandhi, *VLSI Fabrication Principles Silicon and Gallium Arsenide*, John Wiley & Sons, New York, NY, USA, 2nd edition, 1994.

[16] T. Kamins, *Polycrystalline Silicon for Integrated Circuits and Displays*, Kluwer Academic, Dordrecht, The Netherlands, 2nd edition, 1998.

[17] S. Banerjee and S. T. Dunham, "Two Stream model for dopant diffusion in polysilicon incorporating effects of grain growth," in *Proceedings of the Process Physics and Modeling in Semiconductor Technology*, pp. 92–100, Pennington, NJ, USA, 1996.

[18] P. P. Altermatt and G. Heiser, "Predicted electronic properties of polycrystalline silicon from three-dimensional device modeling combined with defect-pool model," *Journal of Applied Physics*, vol. 92, no. 5, pp. 2561–2574, 2002.

[19] D. Inns and P. Campbell, internal communication, 2006.

[20] O. Krause, H. Ryssel, and P. Pichler, "Determination of aluminum diffusion parameters in silicon," *Journal of Applied Physics*, vol. 91, no. 9, pp. 5645–5649, 2002.

[21] P. H. Holloway, "Grain boundary diffusion of phosphorus in polycrystalline silicon," *Journal of Vacuum Science Technology*, vol. 21, no. 1, pp. 19–22, 1982.

[22] H. F. Mataré, "Comments and reply," *Journal of Vacuum Science Technology B*, vol. 1, no. 1, pp. 107–108, 1983.

[23] S. Pearton, J. Corbett, and M. Stavola, *Hydrogen in Crystalline Semiconductors*, Springer, Berlin, Germany, 1992.

[24] N. H. Nickel, W. B. Jackson, and J. Walker, "Influence of grain boundaries on hydrogen transport in polycrystalline silicon," *Journal of Non-Crystalline Solids*, vol. 227–230, pp. 885–889, 1998.

[25] Paul A. Basore, "Numerical modeling of textured silicon solar cells using PC-1D," *IEEE Transactions on Electron Devices*, vol. 37, no. 2, pp. 337–343, 1990.

[26] P. P. Altermatt and G. Heiser, "Development of a three-dimensional numerical model of grain boundaries in highly doped polycrystalline silicon and applications to solar cells," *Journal of Applied Physics*, vol. 91, no. 7, pp. 4271–4274, 2002.